AIAA JOURNAL
Vol. 31, No. 12, December 1993

Early Vortex Burst on a Delta Wing in Pitch

M. R. Soltani* and M. B. Bragg†
University of Illinois at Urbana-Champaign, Urbana, Illinois 61801

Wind-tunnel experiments were performed at a Mach number of 0.13 and Reynolds number of 1.43×10^6 to study the flow over a 70-deg sharp leading-edge delta wing model. The model was tested with the angle of attack static, a sinusoidal oscillation, and a sinusoidal ramp up. Smoke flow visualization of the leading-edge vortices was used as well as six-component balance measurements for the delta wing forces and moments. During the upstroke of a sinusoidal oscillation in pitch the vortex breakdown point was seen to reach the trailing edge at a significantly lower angle of attack than in the static case. However, at large angle of attack, its position lagged that of the static case. The dynamic normal force was less than the static value at angles of attack where the burst point led the static value and was higher when the burst point lagged. A ramped pitch-up motion terminating at 24-deg angle of attack produced lower lift and normal force values when compared to the static values. Furthermore, on cessation of the motion, the dynamic loads did not converge to their static values. This behavior was also attributed to the lead in the burst point position during a pitch-up at low angles of attack.

Nomenclature

C = tunnel test section area, ft^2
C_N = normal force coefficient, N/qS
c = root chord, ft
f = frequency, Hz
K = reduced frequency, $\pi fc/U_\infty$
q = dynamic pressure, lb/ft^2
Re = Reynolds number based on the root chord
S = wing area, ft^2
α = angle of attack, deg
τ = nondimensional time, tU_∞/c

Introduction

MANY modern fighter aircraft have highly swept, low aspect ratio wings to improve their supersonic cruise performance. These aircraft are required to have high levels of maneuvering capability and controllability to be effective in the combat arena. Among these planforms, delta wings and their combinations are the most common. The dominant feature of delta wing flow is the leading-edge vortices which originate at the wing apex and convect downstream over the wing surface. These vortices produce large suction on the wing surface and account for a large portion of the lifting mechanism of delta wings. However, beyond a critical incidence, a sudden transformation takes place and the tightly rolled vortices burst. Both static and dynamic stall are initiated by the breakdown of the leading-edge vortices.

Steady flow over delta wing models and the corresponding aerodynamic forces and moments have been studied by many researchers since the early work of Winter[1] in 1937. A detailed review of the progress made in this area is provided in Ref. 2. The focus of this study is the response of the flowfield over a delta wing when in dynamic motion. Several investigators[3-16] have used flow visualization and/or force measurement techniques to study the complicated flowfield over delta wing models under dynamic oscillatory motion. Their studies have included delta wing models undergoing sinusoidal, linear and sinusoidal ramp, stepwise, and plunging motions about a mean angle of attack. Depending on the wing leading-edge sweep angle, the mean angles of attack were typically selected such that the vortex burst point was located in the vicinity of the wing trailing edge. The models were then pitched about these mean angles of attack up to angles where the leading-edge vortices were burst over the entire, or a large portion of, the wing surface. The following qualitative conclusions highlight some of these findings.

1) For all reduced frequencies tested, $K = 0.01$–0.4, a hysteresis loop in the delta wing normal force and flowfield properties were observed between the increasing and decreasing angle-of-attack conditions.

2) For a low to high angle-of-attack motion, as much as $\alpha = 0$–90 deg, substantial force and moment overshoot and a delay in dynamic stall angle were observed, even for the smallest reduced frequency tested.

3) In the downstroke motion aerodynamic forces and moments were significantly lower than their corresponding static values due to the delay in the re-establishment process of the leading-edge vortices.

4) The magnitude of the overshoot/undershoot and the size of the hysteresis loop depend strongly on the reduced frequency.

5) Unsteady aerodynamic forces and moments are greatly influenced by the mean angle of attack. Increasing the mean angle increases the overshoots of the dynamic loads while enlarging the hysteresis loop.

Unlike the aforementioned studies, in the present investigation the delta wing model was oscillated in pitch from 0- to 55-deg angle of attack, or pitched up in a ramp motion from 0 deg. Therefore, in one oscillation cycle, the flow over the wing surface encountered the formation, breakdown, separation, and reattachment process of the leading-edge vortices. Initially an interesting result was observed in the ramp data; for ramps from 0- to 24-deg angle of attack the normal force coefficient did not return to its static value with time. While investigating this, it was discovered that it could be corroborated by the flow visualization and force data on the static and oscillatory wing. Interestingly, both the flow visualization and force data support the fact that initially the vortex burst point leads the static position when pitch-up is started at 0-deg angle of attack. This paper presents and discusses the measurements supporting this result.

Experimental Procedure

The experiments were conducted in the subsonic wind tunnel located at the Aeronautical and Astronautical Research Laboratory while the authors were at Ohio State University. The open-return tunnel has a test section approximately 5 ft wide,

Received Oct. 6, 1992; revision received May 13, 1993; accepted for publication May 27, 1993.

*Postdoctoral Research Associate, Department of Aeronautical and Astronautical Engineering. Member AIAA.
†Associate Professor, Department of Aeronautical and Astronautical Engineering. Associate Fellow AIAA.

3 ft high, and 8 ft long, and operates at speeds from 0 to 220 ft/s at a Reynolds number of up to 1.3×10^6/ft. The wind-tunnel turbulence level is less than 0.1%.

Model

The model was a simple flat plate delta wing of 70-deg leading-edge sweep, a 20.61-in. root chord, and a 15-in. span at the trailing edge. The wing was constructed of 0.25-in.-thick aluminum (0.012 thickness to chord ratio). To leave the leeward side (upper surface) flat, the leading and trailing edges were chamfered on the windward side (lower side) of the wing at 14 deg. A pod large enough to house the balance and necessary hardware was attached under the wing. Figure 1 shows a drawing of the model. The flow visualization was conducted using a slightly different model. This model was 0.50 in. thick and the leading edge was sharpened using a 25-deg bevel from the top and bottom surface.[2]

Oscillation System

A system was designed that pitched the model through large-amplitude oscillations. Figure 2 shows a schematic drawing of this apparatus mounted underneath the wind-tunnel test section. The oscillation system uses a belt and pulley arrangement to drive a cam that produces the sinusoidal pitch motion of the model. The model was attached to the system by a push rod and a strut arrangement as shown in Fig. 2. Model oscillation was from 0- to 55-deg angle of attack and of the form

$$\alpha(t) = 55 - 27.5[1 + \cos(2\pi ft)]$$

A computer-controlled solenoid clutch assembly was installed in the belt reduction system. This allowed the cam to be rapidly connected or disconnected from the motor drive system. Thus, sinusoidal ramp-up and ramp-down motions could be generated at various frequencies using segments of the sinusoidal motion. A potentiometer mounted on the arm of the oscillation system provides the instantaneous angle of attack of the model during both the static and dynamic motions. Detailed information about the oscillation system used in this investigation can be found in Ref. 2.

Force and Tare Measurements

Force measurements were made using a six-component internal strain-gauge balance. There are two types of force and moment tares acting on the balance. The gravitational loads due to the model and metric balance weight are functions of the angle of attack and the inertial forces and moments produced by the moments of inertia of the oscillating model and metric balance. These loads can be measured when the model is oscillating in still air, the wind-off tests. Both of these forces and moments have been measured and subtracted from the wind-on data.

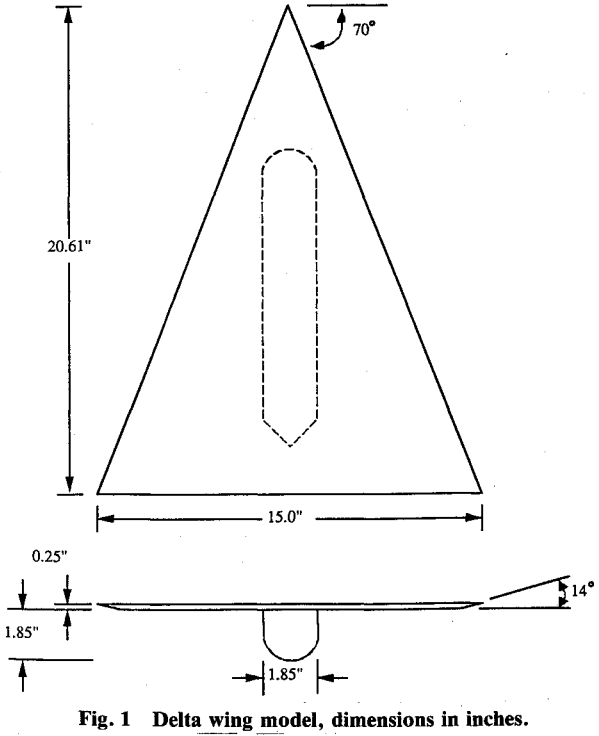

Fig. 1 Delta wing model, dimensions in inches.

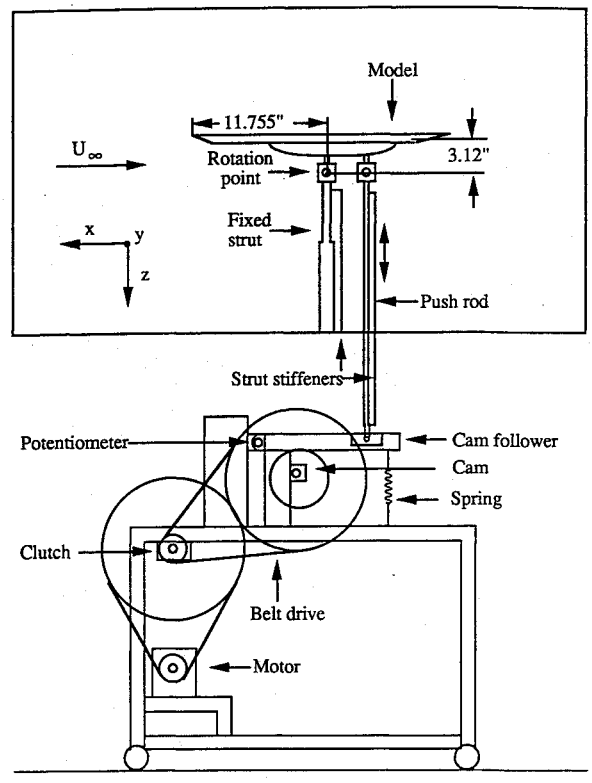

Fig. 2 Oscillation system, not to scale.

Data Acquisition and Reduction

Dynamic oscillation data presented in this paper are an average of at least 10 cycles taken at a sample rate of 100 Hz at the lowest reduced frequency increasing to 750 Hz at the highest reduced frequency. The ramp motion data are an average of at least two different runs at the same tunnel speed, data sample rate, and nondimensional pitch rate. Raw data for all of the reduced frequencies and nondimensional pitch rates were saved unfiltered on a personal computer. These data were later digitally filtered and reduced to forces and moments as a function of time.

Blockage corrections at small angle of attack were determined by the method of Ref. 17 and were found to be small relative to all of the aerodynamic variables. Thus, in all of the calculations, no blockage correction was applied. In addition, Ref. 18 suggests that blockage ratios (S/C, wing area/test section area) of less than 7% can usually be considered negligible. The blockage ratio for this investigation was 7.1%. Currently, there are no methods available which can accurately estimate the blockage corrections at the high angles of attack of this study. The data were corrected for the presence of the support strut by the "image" support system method[2] as described in Ref. 17.

Flow Visualization

Flow visualization was used to document the leading-edge vortices before, during, and after bursting under both static and dynamic conditions. These tests were conducted at a free-stream velocity of approximately 15 ft/s, $Re = 0.16 \times 10^6$. The smoke was injected into the flow near the wing vertex. Refer-

ence 2 shows a detailed drawing of the setup and discusses the operation of the smoke flow generator. Leading-edge vortices were illuminated using high intensity lamps. A VHS video tape camera was used to record the vortices formed on the suction side of the model.

Photographs provided in this study were taken from a video monitor by freezing the desired frame and photographing the screen. The breakdown location of the vortices was measured from the photographs or directly from the monitor. The flow-visualization portion of this study was conducted as an aid in interpreting the force and moment data. It was not originally intended to provide a detailed quantitative documentation of the burst point location. However, the burst point location data have been carefully obtained from the video and compare favorably to data by other researchers on similar wings. An exact location of the breakdown point is extremely hard to obtain from the flow visualization. There always exists an inaccuracy which should be taken into account when comparing different results.[19] This is due to the fact that vortices do not burst instantaneously, as discovered by Lambourne and Bryer.[3] Therefore, to locate the burst point, a judgment must be made by the observer as to what point the vortices are considered to be burst.[19] The accuracy of these data are adequate to show the early burst phenomenon discussed later.

Error Analysis

The uncertainty in the experimental data was estimated based on the methods in Ref. 20. The sources of errors associated with the balance data include errors due to the balance calibration, analog-to-digital (A/D) conversion, and system noise. The A/D and system noise errors were minimized by averaging several hundred samples for the static case and several cycles of data for the oscillatory or ramp data. Furthermore, the averaged dynamic data were digitally filtered, thus reducing the noise. For the six-component balance, the total system error is estimated to be less than 0.7% of the full-scale load for each component. For the normal beam, this becomes a maximum error in C_N of ± 0.035 at the test dynamic pressure.

The parallax error in the vortex burst location from the flow-visualization data was estimated. This error is caused by the stationary camera location, which causes the camera orientation with respect to the delta wing model to change with angle of attack. For the worst case, and using the vortex height data from Ref. 21, the maximum error in vortex burst location is $\Delta x/c = 0.02$.

Results and Discussion

The effect of large amplitude pitching motion on the flowfield and the aerodynamic characteristics of a three-dimensional lifting surface was extensively studied. The experiments were performed on a 70-deg sharp leading-edge delta wing model at a Reynolds number of 1.43×10^6. Data were taken during forced sinusoidal oscillations and ramps at various reduced frequencies including the static (zero frequency) case. Comparison of the static and dynamic flow-visualization results taken at a Reynolds number of 0.16×10^6 revealed an interesting early vortex burst phenomenon at low angles of attack, which is the subject of this paper. The balance of the data taken at a higher Reynolds number further supported these findings. Detailed analysis of other aspects of this test, including the effect of Reynolds number and reduced frequency, can be found in Ref. 2.

Static Tests

Figure 3 shows the static variation of the vortex breakdown location with angle of attack obtained from flow visualization at a chord Reynolds number of 0.16×10^6. To see the hysteresis in the breakdown position, the data for both increasing and decreasing angle of attack are shown in this figure. As previously indicated, the breakdown location was measured frame by frame from the smoke flow-visualization video.

The static data shown in Fig. 3 reveal similar trends with those obtained by other researchers[4–7] who used a slightly different method in measuring the breakdown position. The presence of a small hysteresis in the burst location between increasing and decreasing angle of attack, seen in Fig. 3, was also noted by Lowson[5] and LeMay et al.[6] This figure indicates that to move the breakdown position into the wake, the angle of attack when α is decreasing should be less than the corresponding angle at which the burst point moved onto the wing surface with increasing α. The reason for this phenomenon is not yet clear. For $x/c < 0.1$, the local wing span is very small. This makes it very difficult to distinguish the two vortices from one another. As a result, it is extremely difficult, if not impossible, to differentiate between the burst and unburst vortices. For this reason, for $x/c < 0.1$, the vortex breakdown locations were not measured in this study or for other studies[4,6,9,21] in the literature.

Dynamic Tests

The 70-deg aluminum delta wing model was sinusoidally oscillated in pitch from 0- to 55-deg angle of attack at various reduced frequencies. In the following sections, results for the oscillatory motion will be examined first. Dynamic data for the ramp type motion will be presented in the subsequent section.

Figure 4 shows the smoke flow over the wing surface for the oscillatory pitch-up motion at two different angles of attack, 25 and 35 deg, for a reduced frequency of 0.09 and compares them with those of the static case at the same angles of attack. This figure illustrates the basic flow features over a delta wing model, the presence of the two strong leading-edge vortices and the breakdown phenomenon. Comparison of the smoke flow over the wing surface for both static and dynamic cases at 25-deg angle of attack shows an increase in the diameter of the leading-edge vortices in the vicinity of the trailing edge for the dynamic case, Fig. 4a, which indicates the breakdown of the vortices.

It is believed that in the dynamic motion the breakdown point at any angle of attack lags its static position; however, the flow-visualization results shown in Fig. 4 contradict this. For an angle of attack of 25 deg, Fig. 4a clearly shows that the vortices over a portion of the oscillatory wing are burst, with the burst point located at about 80% of the wing root chord. (Note that the wing is marked with a spanwise line every 10% root chord.) For this incidence the vortices for the static case are still unburst, Fig. 4b. For the static case, the burst point moves onto the wing surface at an incidence of about 28 deg.

As the angle of attack is further increased, the breakdown point for the oscillatory wing moves toward the wing apex, reaching about 60% of the wing root at an incidence of 35 deg, Fig. 4c. For the static case at this angle of attack, Fig. 4d shows that the burst point is located at about 40% of the wing

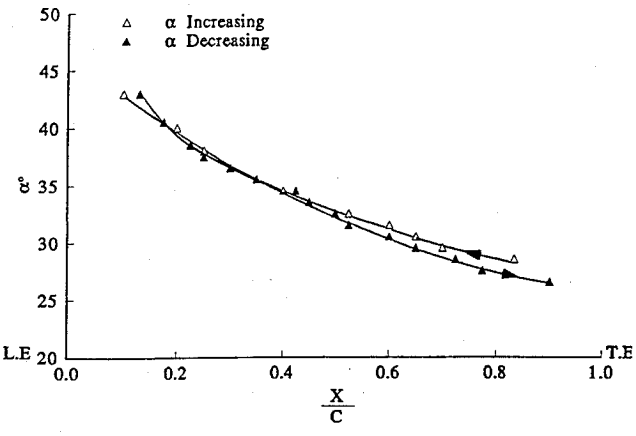

Fig. 3 Variation of the static vortex breakdown location with angle of attack.

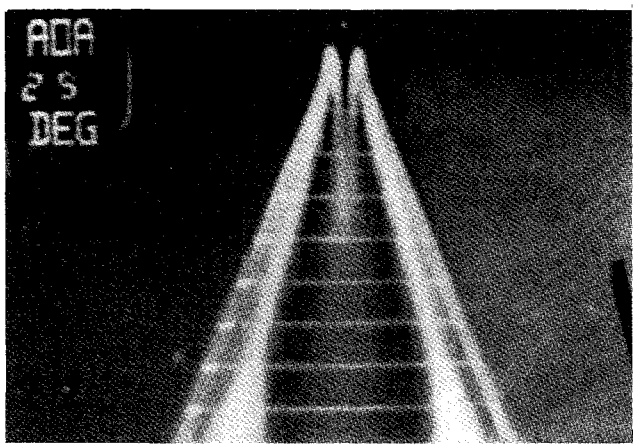

a) Dynamic pitch-up, $K = 0.09$, $\alpha = 25$ deg

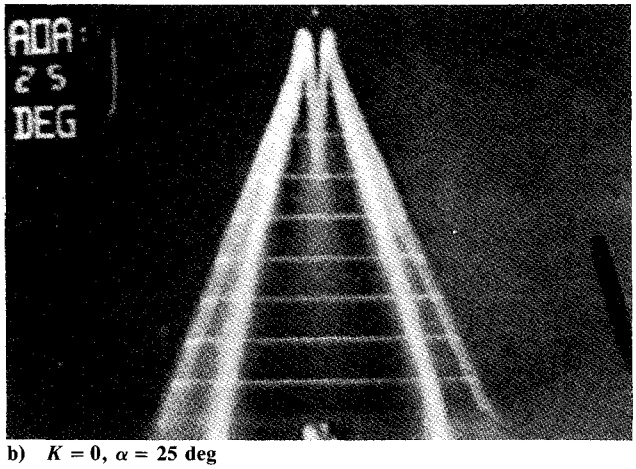

b) $K = 0$, $\alpha = 25$ deg

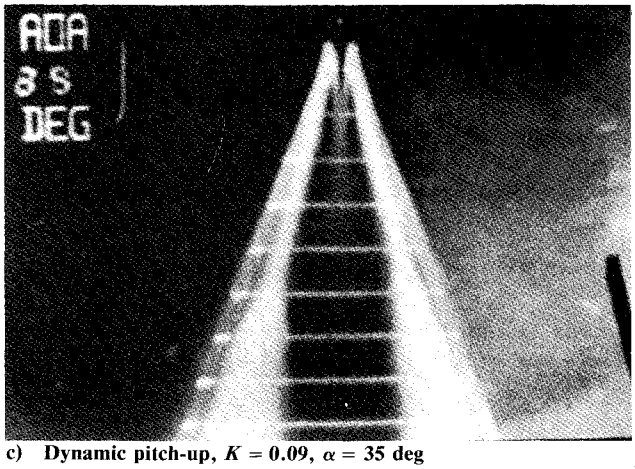

c) Dynamic pitch-up, $K = 0.09$, $\alpha = 35$ deg

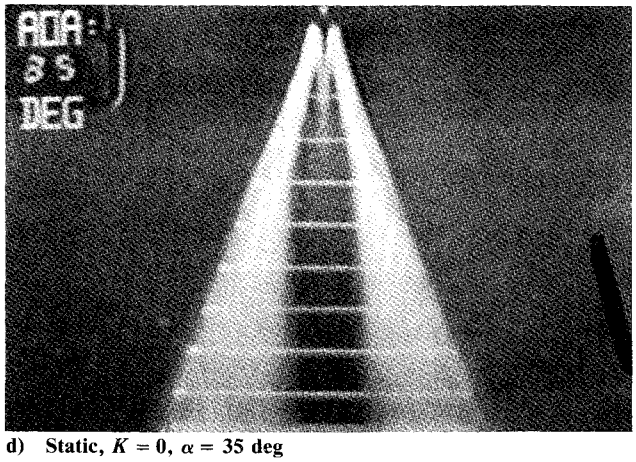

d) Static, $K = 0$, $\alpha = 35$ deg

Fig. 4 Smoke flow visualization for the static and dynamic pitch-up, $Re = 0.16 \times 10^6$.

root chord, leading that of the dynamic case, Fig. 4c. Therefore, from the present flow-visualization result it is seen that there exists a range of angles of attack where the breakdown point for the dynamic motion leads its static location. However, for higher angles of attack, the dynamic burst point lags its static position as seen from Fig. 4.

The burst location data over the entire range of angles of attack are summarized in Fig. 5. This figure shows the variation of the dynamic vortex breakdown location over the wing surface vs angle of attack for a reduced frequency of 0.09. Static data for increasing α are also shown for comparison. As in the static case, the dynamic breakdown locations were measured from the smoke flow-visualization photographs, some of which are shown in Fig. 4. From Fig. 5 note that during the upstroke motion the dynamic burst point moves onto the wing surface at a lower angle of attack than that of the static case. During the pitch-up motion, the burst point moves onto the wing surface at an incidence of about 18 deg, 10 deg less than that of the static case. At an angle of attack of about 30 deg, the breakdown points for the dynamic pitch-up motion and the static case are located at the same chord-

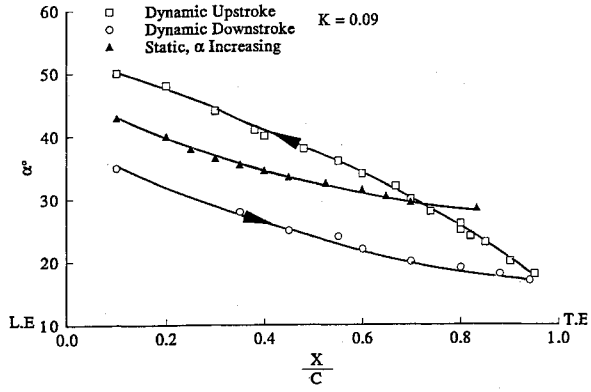

Fig. 5 Dynamic vortex breakdown location.

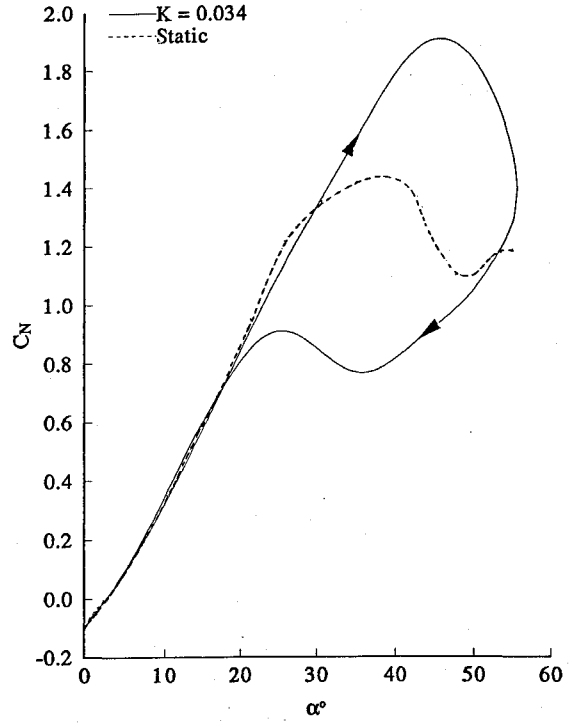

Fig. 6 Comparison of static and dynamic normal force coefficient.

wise station on the wing surface. Beyond this incidence, the dynamic burst point lags its static location, and the magnitude of the lag increases as higher α are reached, Fig. 5.

From Fig. 5, it is clearly seen that in the pitch-down motion, the leading-edge vortices remain burst over the wing surface until the angle of attack is reduced to about 35 deg. This large lag in the vortical flow reformation is associated with the persistence of the separated wake-like flow, as well as the fast variation of the angle of attack, $f = 2.17$ Hz. At an incidence of about 18 deg, the dynamic burst point for the pitch-down motion is located at the same chordwise station on the wing surface as it was during the pitch-up motion, about 94% of the wing root chord, Fig. 5. This may indicate that for the dynamic motion, the burst point moves off the wing surface at approximately the same angle of attack as it moved onto the wing surface during the pitch-up motion. For the static case, however, the trend was quite different where the hysteresis in burst point location between upstroke and downstroke was largest when the burst point was in the vicinity of the trailing edge.

Figure 6 compares the static and dynamic variation of the normal force coefficient with angle of attack for a reduced frequency of $K = 0.034$. Between 20- and 30-deg angle of attack the dynamic C_N data are slightly less than their corresponding static values. This could be related to the breakdown of the leading-edge vortices moving onto the wing surface at lower angle of attack, $\alpha = 18$ deg, for the oscillatory motion case, Fig. 5. For the static case, vortex breakdown reached the trailing edge at an incidence of about 28 deg, Fig. 3. Note that the dynamic and static C_N are equal at about 31-deg angle of attack, from Fig. 5 this corresponds approximately to the position where the burst locations for both cases, static and dynamic, are at the same chordwise station. Thus, the normal force in the dynamic case is lower than the static value over the angle-of-attack range where early bursting was observed in the dynamic flow-visualization data.

Surface-pressure results of Ref. 8, taken at a reduced frequency of $K = 0.0764$ over a range of motion of 2–60 deg, showed that in the upstroke motion static-pressure coefficients on the upper surface at the 75% chord location were slightly lower than those of the static case for α of 20–35 deg. The increase in the pressure coefficients for this angle-of-attack range might be related to the early breakdown phenomenon observed in our flow-visualization results. The authors of Ref. 8, however, do not mention this increase in the pressure for the dynamic case in their paper. Note that the delta wing model used in Ref. 8 is similar to the one used in the present investigation.

At about 30-deg angle of attack, the lead in the dynamic vortex burst point vanishes, Fig. 5, and with further increase of the incidence, the dynamic burst location lags its static position, producing higher normal force. The normal force coefficient for this reduced frequency reached its maximum value of approximately 1.9 at about 46-deg angle of attack. For the static case, the maximum normal force coefficient occurs at an incidence of about 38 deg, about 8 deg lower than the corresponding value when in dynamic motion. This is clearly an indication of the lag in the breakdown location during the dynamic upward motion, resulting in higher normal force. During the rest of the cycle, $\alpha = 46$–55 deg, the normal force coefficient decreases substantially, indicating further deterioration of the leading-edge vortices and flow separation.

The flowfield when the model is in the downstroke motion is not the focus of this paper. However, it further demonstrates the relationship between the vortices as shown by the flow visualization and the normal force and will be discussed briefly here. In the downstroke motion, the dynamic normal force coefficient, for angles of attack of 52 deg and below, is smaller than its corresponding static value until an incidence of about 18 deg is reached, Fig. 6. For this part of the motion, $\alpha = 52$–18 deg, the flow re-establishment process is very slow due to the persistence of the separated flow produced at the end of the pitch-up motion. The normal force coefficient decreases as α is reduced until an incidence of about 36 deg beyond which C_N starts to increase, Fig. 6. This corresponds to the angle where the vortices were again visible in the flow visualization near the leading edge. In Fig. 5 the leading-edge vortex burst point was at approximately $x/c = 0.10$ at 36-deg angle of attack. At an angle of attack of about 18 deg, C_N reaches the same value it had in the upstroke motion as the flowfield becomes fully re-established, Fig. 6. Remember 18 deg was the angle of attack where the vortex burst point was at approximately the same position on the wing trailing edge on the upstroke and downstroke.

Figure 6 also shows that in the pitch-down motion the normal force coefficient for angles of attack of approximately 18–8 deg is slightly higher than the corresponding values in the upstroke motion. This creates a counterclockwise hysteresis loop. Note that the hysteresis loop formed at moderate-to-high angles of attack has a clockwise direction. Therefore, the two hysteresis loops together form a distorted figure eight shape. This low angle-of-attack hysteresis was also noted by other researchers.[8,9] The reason for this phenomenon is not yet clear and could not be discerned from the flow visualization.

Ramp Motion

Figure 7 shows the variation of the normal force coefficient vs τ, time nondimensionalized by convective time, for the ramp motions from 0- to 24-, 38-, 47-, and 55-deg angle of attack and at a nondimensional pitch rate of $K = 0.034$. Note that the ramp motion used in this investigation is derived from a section of a continuous oscillatory motion of frequency f. Therefore, the usual reduced frequency K will be used to describe the ramp pitch rate and will be referred to in this study as the nondimensional pitch rate. The model angle of attack is shown vs τ in the lower part of Fig. 7. Static data for 24-, 38-, 47-, and 55-deg angle of attack are also shown for comparison. The overshoot in the ramp normal force data caused by the convective time lag of the adjusting flowfield is apparent. Figure 7 shows that for the ramp motions of 0–47 and 0–55 deg, maximum normal force coefficients occur at the

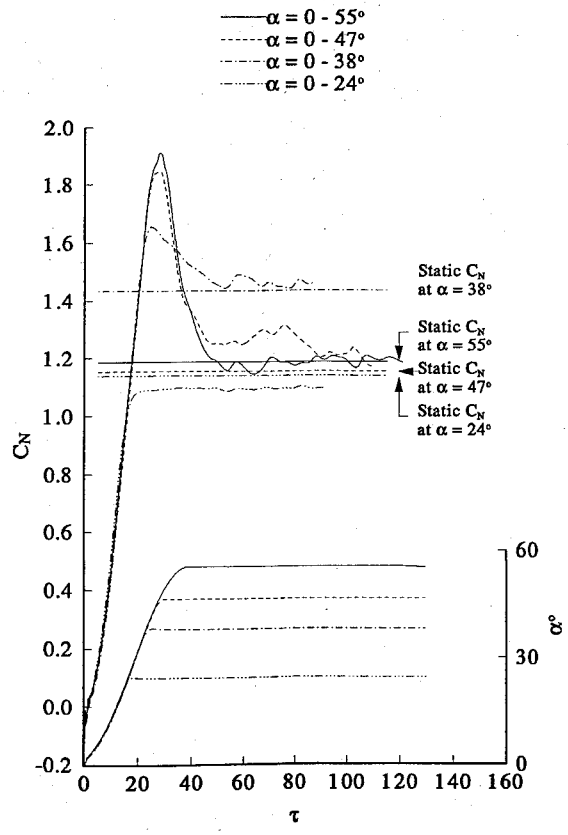

Fig. 7 Effect of ramp maximum angle of attack on the normal force coefficient, $K = 0.034$.

same angle of attack to within 0.5 deg, at $\alpha = 47$ deg, although the magnitudes of $C_{N_{max}}$ for both cases are not the same. For the 0–55-deg ramp motion, $C_{N_{max}}$ is slightly higher than that of the 0–47-deg ramp.

For the 0–38-deg pitch-up, $C_{N_{max}}$ is obtained after the model has reached 38-deg angle of attack. The nondimensional time required for the model to return to the static value, once the dynamic $C_{N_{max}}$ has been reached, varies with the maximum angle of attack, Fig. 7. From this figure it is clearly seen that for the 0–55-deg ramp motion the time lag is smaller than for the other two cases.

For the 0–24-deg ramp motion case, Fig. 7 shows that again $C_{N_{max}}$ is obtained after the model has reached an angle of attack of 24 deg. In addition, dynamic $C_{N_{max}}$ is seen to be less than its corresponding static value at 24-deg angle of attack. This is very interesting and correlates well with the oscillatory data of Fig. 6 and the flow visualization results of Figs. 4 and 5. Figure 6 showed that in the upstroke motion the dynamic normal force coefficient for angles of attack of 20–30 deg is slightly less than that of the static case. Figure 5 showed that the vortex burst point moved onto the wing at 18-deg angle of attack during pitch-up but not until 28 deg in the static case.

The ramp motions used in this investigation are all derived from sections of a continuous oscillatory motion. Therefore, measurements have shown that for ramps starting at 0-deg angle of attack, the aerodynamic forces and moments for the ramp motion are the same as those of the oscillatory case while in the upstroke motion.[2] As a result, the flowfield over the oscillatory model for increasing α will be similar to that of the ramp motion case. Therefore, the data of Fig. 5 for the dynamic upstroke case can be used to locate the breakdown point for the ramp motion. Thus, when the model is pitched from 0- to 24-deg angle of attack, the leading-edge vortices will experience breakdown over the model. Figure 5 shows that at 24-deg angle of attack, the burst point for the oscillatory wing is located at about 83% of the wing root chord. Accordingly, the lower dynamic $C_{N_{max}}$ seen in Fig. 7 is due to the early bursting of the leading-edge vortices at low angle of attack.

Figure 7 also shows that for the 0–24-deg ramp case, on cessation of the motion, the dynamic values did not converge to their static values as they did for the other cases. This could be related to the persistence of the burst vortices over the wing surface. Note that for the static case, the vortex burst point reached the wing trailing edge at an incidence of approximately 28 deg when α was increasing, Fig. 3. However, when α was decreasing, the burst point moved off the wing surface at an incidence of about 26 deg. It appears that once the breakdown moved onto the wing surface, it remained stable over the wing unless the incidence was reduced. Previous investigators[5,6] have shown that for the static case the angle at which bursting moved onto the wing surface was always greater than the angle required to move the breakdown point off the model and into the wake. Figure 3 clearly supports these findings. Thus, even in the static case, the vortex burst point tends to remain on the wing once it has moved onto the wing unless the angle of attack is reduced.

As the model is pitched up to 24-deg angle of attack, the burst point moves onto the wing surface before the motion is terminated, about 18 deg for $K = 0.09$, see Fig. 5. To move the breakdown point off the wing surface, the angle of attack would have to be reduced, which is not the case in the pitch-up and hold situation. Therefore, the vortices will remain burst over the wing surface resulting in a lower normal force coefficient when compared to the corresponding static values at 24-deg angle of attack, see Fig. 7.

Summary and Conclusions

An extensive experimental study was conducted to investigate the flow on a 70-deg sharp leading-edge delta wing model undergoing large amplitude pitching oscillations. Ramp motions were produced using an initial sinusoidal increase in angle of attack and hold. Unlike most other studies, the model was oscillated or pitched from 0-deg angle of attack. Thus each ramp or oscillation experienced the initial formation, growth, and bursting of the leading-edge vortices. Because of this motion, an interesting phenomenon was observed.

During the upstroke motion the vortex breakdown point was seen to reach the model trailing edge at a smaller angle of attack than it did in the static case. This phenomenon was observed from the flow-visualization result. Furthermore, the dynamic normal force data for moderate angles of attack, 20–30 deg, were slightly less than their corresponding static values. This further confirmed the flow-visualization results. However, at higher angles of attack, the flow visualization showed the burst point lagging the static values and the forces were greater than the static values. This high-angle-of-attack behavior was the usual burst point lag and force overshoot often measured and reported.

Terminating the ramp motion at 47- or 55-deg angle of attack produced almost identical results, although slightly larger normal force overshoots for the 0–55-deg case. The ramp to 38 deg produced significantly lower overshoots. The time to return to the static value decreased slightly as the maximum ramp angle was increased.

However, for the 0–24-deg ramp motion case, the delta wing model produced lower normal force values when the data were compared to the static case. Furthermore, upon cessation of the model motion, the dynamic loads did not converge to their static values as they did for other ramp motions. This is also believed to be due to early movement of the vortex burst point onto the wing during the pitch-up. The persistence of the burst point to remain on the wing prevents the model from attaining the static lift value after the motion has stopped.

References

[1]Winter, H., "Flow Phenomena on Plates and Airfoils of Short Span," NACA TM, 798, 1937.

[2]Soltani, M. R., "An Experimental Study of the Relationship Between Forces and Moments and Vortex Breakdown on a Pitching Delta Wing," Ph.D. Dissertation, Dept. of Aeronautical and Astronautical Engineering, Univ. of Illinois, Urbana-Champaign, IL, 1992.

[3]Lambourne, N. C., and Bryer, D. W., "The Bursting of Leading-Edge Vortices—Some Observations and Discussion of the Phenomenon," Aeronautical Research Council, Reports and Memoranda, 3282, April 1961.

[4]Wentz, W. H., and Kohlman, D. L., "Vortex Breakdown on Slender Sharp-Edged Wings," AIAA Paper 69-778, July 1969.

[5]Lowson, M. V., "Some Experiments with Vortex Breakdown," *Journal of the Royal Aeronautical Society,* Vol. 68, May 1964.

[6]LeMay, S. P., Batill, S. M., and Nelson, R. C., "Leading-Edge Vortex Dynamic on a Pitching Delta Wing," M.S. Thesis, Univ. of Notre Dame, Nag-1-727, South Bend, IN, April 1988.

[7]Thompson, S., Batill, S., and Nelson, R., "The Separated Flow Field on a Slender Delta Wing Undergoing Transient Pitching Motion," AIAA Paper 89-0194, Jan. 1989.

[8]Thompson, S. A., Batill, S. M., and Nelson, R. C., "Delta Wing Surface Pressures For High Angle of Attack Maneuvers," AIAA Paper 90-2813, Aug. 1990.

[9]Jarrah, A. M., "Low-Speed Wind-Tunnel Investigation of Flow About Delta Wings, Oscillating in Pitch to Very High Angles of Attack," AIAA Paper 89-0295, Jan. 1989.

[10]Sawyer, R., and Sullivan, J., "Lift Development of Delta Wing Undergoing Constant Acceleration from Rest," AIAA Paper 90-0310, Jan. 1990.

[11]Soltani, M. R., Bragg, M. B., and Brandon, J. M., "Measurements on an Oscillating 70-Degree Delta Wing in Subsonic Flow," *Journal of Aircraft,* Vol. 27, No. 3, 1990, pp. 211–219.

[12]Bragg, M. B., and Soltani, M. R., "Measured Forces and Moments on a Delta Wing During Pitch-Up," *Journal of Aircraft,* Vol. 27, No. 3, 1990, pp. 262–267.

[13]Robinson, M. C., Wissler, J. B., and Seiler, F. J., "Unsteady Surface Pressure Measurements on a Pitching Rectangular Wing," AIAA Paper 88-0328, Jan. 1988.

[14]Brandon, J. M., and Shah, G. H., "Unsteady Aerodynamic Characteristics of a Fighter Model Undergoing Large-Amplitude Pitching Motion at High Angles of Attack," AIAA Paper 90-0309, Jan. 1990.

[15]O'Leary, C. O., Weir, B., and Walker, J. M., "Measurement of Derivatives Due to Acceleration in Heave and Sideslip," AGARD-CP-496, May 1991, pp. 9-1–9-11.

[16]Robinson, M. C., Seiler, F. J., and Wissler, J. B., "Pitch Rate and Reynolds Number Effects on a Delta Wing Undergoing Large Amplitude Pitching Motions," AIAA Paper 88-2577, June 1988.

[17]Rae, W. H., and Pope, A., *Low-Speed Wind Tunnel Testing,* 2nd ed., Wiley, New York, 1984, Chap. 6.

[18]Pass, C. Q., "A Wake Blockage Correction Method for Small Subsonic Wind-Tunnels," AIAA Paper 87-0294, Jan. 1987.

[19]Nelson, R. C., "The Role of Flow Visualization in the Study of High-Angle-of-Attack Aerodynamics," *Tactical Missile Aerodynamics,* edited by M. J. Hemsch and J. N. Nielsen, Vol. 104, Progress in Astronautics and Aeronautics, AIAA, New York, 1986, pp. 43–88.

[20]Coleman, H. W., and Steele, W. G., *Experimentation and Uncertainty Analysis for Engineers,* Wiley, New York, 1989.

[21]Payne, F. N., "The Structure of Leading Edge Vortex Flows Including Vortex Breakdown," Ph.D. Dissertation, Dept. of Mechanical and Aerospace Engineering, Univ. of Notre Dame, South Bend, IN, 1987.